Electronic Supplementary Information

High Sensitivity Terahertz Metamaterial Sensor for Trace Pesticide Detection

Fardin Ahmed[a], Md Ayenul Azim[a], Ahmed Zubair[a,*]

[a] Department of Electrical and Electronic Engineering, Bangladesh University of Engineering and Technology, Dhaka 1205, Bangladesh
[*] ahmedzubair@eee.buet.ac.bd

S1. TRANSMISSION AND REFLECTION COEFFICIENT

The Fig. S1 shows the S_{21} parameter (in dB) across 0–2.5 THz, with consistently low values below -80 dB, indicating minimal wave transmission through the structure. A sharp dip near 2 THz marks a resonance where transmission is further suppressed due to strong electromagnetic interactions. The low transmission is attributed to the width of the structure being greater than the depth of the skin, effectively blocking incident waves. Near 1.25 THz, a sudden change in the normalized impedance is observed, which can be attributed to the behavior of the reflection coefficient S_{11}. At this frequency, $S_{11} \approx 1 + 0j$, indicating nearly total reflection with no phase shift of the incident wave. The effective impedance (Z_{eff}) of the absorber can be determined using the relation:

$$Z_{\text{eff}} = \frac{1 + S_{11}}{1 - S_{11}}. \tag{S1}$$

Given that $S_{11} \approx 1$, the denominator of this expression approaches zero, resulting in a very high Z_{eff}. This abrupt increase in the imaginary part of the impedance signifies a transition in the electromagnetic response of the absorber, from capacitive to inductive behavior.

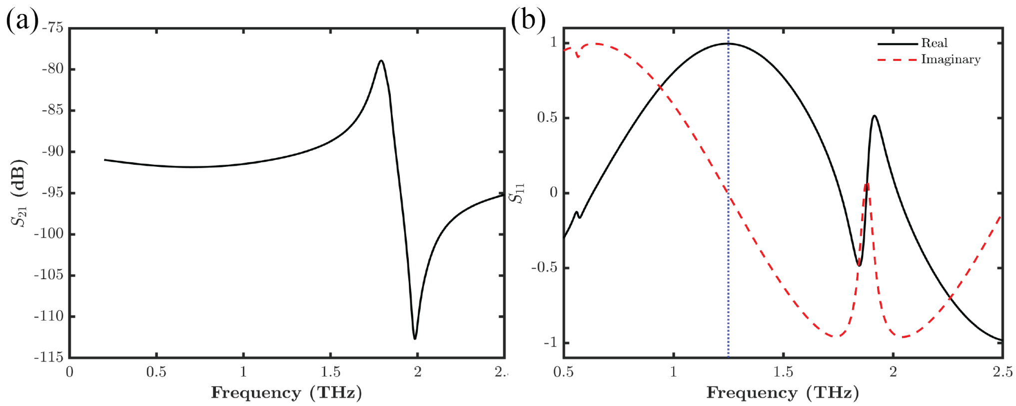

Fig. S1. (a) Transmission coefficient S_{21} and (b) reflection coefficient S_{11}.

S2. SURFACE CURRENT, ELECTRIC FIELD AND MAGNETIC FIELD ANALYSIS AT NON-RESONANT FREQUENCY

At the non-resonant frequency, the electromagnetic response of the unit-cell structure is significantly weaker, as evidenced by the electric field, surface current, and magnetic field distributions. The electric field intensity is notably reduced, with minimal localization around the split gaps and resonator arms, indicating a lack of strong capacitive effects or charge accumulation. The surface current distribution in both the top and bottom layers appears disorganized, with no pronounced directional flow to establish effective dipole interactions. Additionally, the magnetic field generated at this frequency is weak, and the surface current vectors lack coherence, failing to exhibit the anti-parallel flow necessary for significant magnetic coupling or impedance matching. These observations highlight the absence of strong electromagnetic interactions, resulting in reduced absorption and diminished field coupling compared to resonant conditions.

S3. ANALYTICAL DERIVATION OF EQUIVALENT CIRCUIT PARAMETERS

The equivalent circuit parameters were initially derived using analytical expressions that relate inductance and capacitance to the geometric parameters of the metamaterial structure. Specifically, the inductance of each ring element was estimated using the following formula [1]:

$$L = \mu_0 \cdot r_{\text{avg}} \left[\ln \left(\frac{8 r_{\text{avg}}}{w} \right) - 0.5 \right] \tag{S2}$$

where μ_0 is the permeability of the free space, r_{avg} is the average radius of the ring, and w is the width of the conductor. The capacitance of the split gap in the resonator was calculated as,

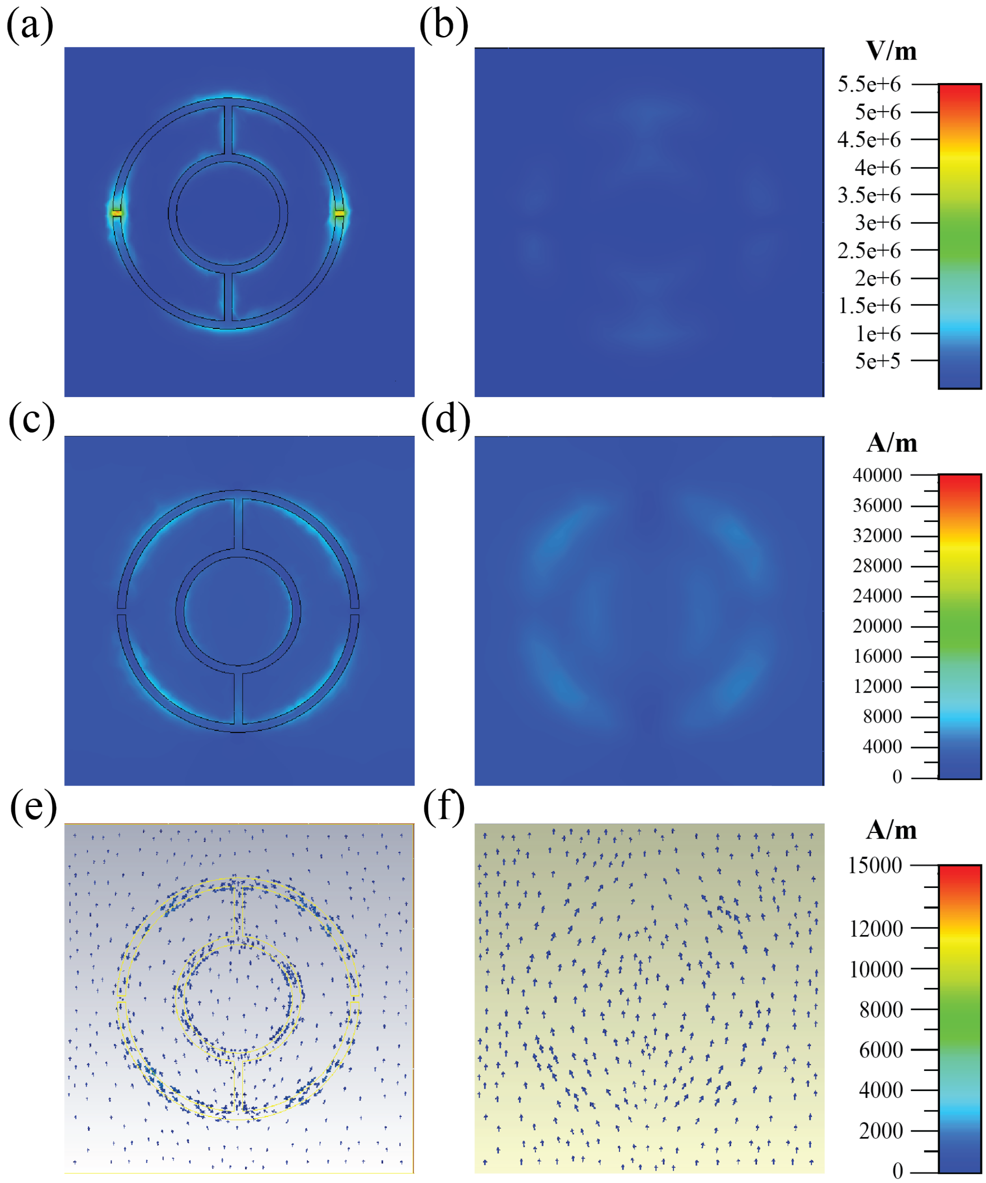

Fig. S2. Electric field distributions of (a) front side and (b) back side of the structure. Magnetic field distribution of (c) the front side and (d) the back side of the structure. The surface current distribution is shown for (e) the front side and (f) the back side.

$$C_{\text{gap}} = \frac{\varepsilon_0 \varepsilon_r w h}{g} \tag{S3}$$

with ε_0 being the vacuum permittivity, ε_r the relative permittivity of the substrate, h the thickness of the conductor, and g the size of the gap. The accumulation of the electric field between the two concentric rings gives rise to a capacitive effect. The coupling capacitance between the two rings was estimated as follows[2],

$$C_{\text{coupling}} = \frac{2\pi \varepsilon_0 \varepsilon_r h}{\ln\left(\frac{o_r}{i_r}\right)} \tag{S4}$$

where i_r and o_r are the inner and outer radii of the concentric resonant structures, respectively.

In our model, the split gap capacitance (C_{gap}) and the coupling capacitance ($C_{coupling}$) contribute to the effective capacitance (C_{eff}) of the metamaterial structure, which in turn determines the resonance frequency via:

$$f_0 = \frac{1}{2\pi\sqrt{L_{eff}C_{eff}}}, \tag{S5}$$

where L_{eff} and C_{eff} are the effective inductance and capacitance, respectively, of the equivalent resonator.

These initial analytical estimates served as the starting point for iterative optimization in the Advanced Design System (ADS). The circuit parameters were fine-tuned to achieve close alignment between the equivalent circuit's reflection coefficient and the full-wave simulation results from CST.

S4. DETECTION OF SPECIFIC PESTICIDES IN WHEAT FLOUR USING RESONANCE AND ABSORBANCE SHIFTS

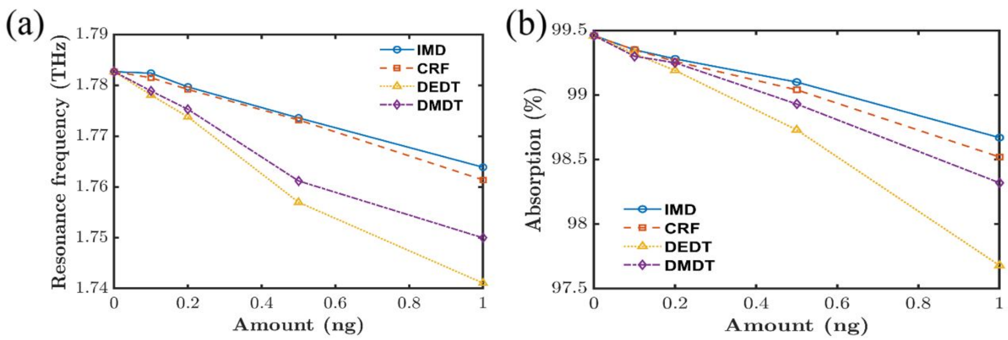

Fig. S3. (a) Resonance frequency and (b) absorbance versus concentration for four pesticides.

The metamaterial sensor developed in this study can effectively detect and identify specific pesticides present in samples such as wheat flour by analyzing changes in resonance frequency and absorbance. As shown in Fig S3(a), each pesticide—Imidacloprid (IMD), carbofuran (CRF), N, N-diethyldithiocarbamate sodium salt trihydrate (DEDT), and N, N-dimethyldithiocarbamate sodium salt hydrate (DMDT)—induces a characteristic shift in the sensor's resonance frequency depending on its concentration. Similarly, Fig. S3(b) demonstrates that absorbance decreases uniquely for each pesticide as the amount increases. When a contaminated wheat flour sample is introduced to the sensor, the interaction between the pesticide residues and the sensor surface alters the local electromagnetic environment. This change results in a measurable shift in both the resonance frequency and absorbance. By comparing these shifts with the known response patterns of individual pesticides, one can determine not only the presence of contamination but also identify which specific pesticide is present. Each pesticide has a distinct response curve, acting as a spectral signature. Analyzing the measured data from an unknown sample against these known signatures makes it possible to match the observed changes with a particular pesticide. Advanced data processing techniques, such as multivariate regression or machine learning classification models, can enhance accuracy, especially in complex or mixed-contaminant scenarios. This approach enables reliable, real-time detection of specific pesticide residues in wheat flour without chemical labeling or complex sample preparation, offering a powerful tool for food safety and quality control.

S5. EFFECT OF SPLIT GAP VARIATION ON RESONANT CHARACTERISTICS

We conducted a detailed analysis of the effect of varying the split gap on the magnetic field distribution and resonance frequency to investigate the observed nonlinearity in frequency behavior. As the split gap increases from 0.8 µm to 1.0 µm, the resonance frequency exhibits a non-smooth, abrupt shift, rather than a gradual change. As shown in Fig. S4, this shift is accompanied by a significant reduction in the magnetic field strength, where the peak magnetic field drops from approximately 80,000 A/m (at 0.8 µm) to 40,000 A/m (at 1.0 µm). This 50%

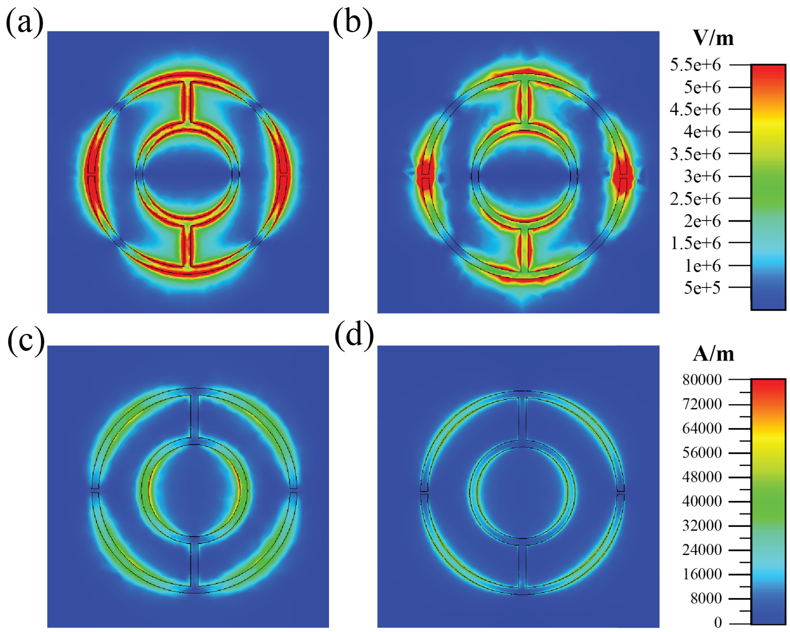

Fig. S4. Electric field distribution when the split gap is (a) 0.8 µm and (b) 1 µm of the structure. Magnetic field distribution when the split gap is (c) 0.8 µm and (d) 1 µm.

decrease in magnetic field intensity is primarily attributed to the reduction in capacitance due to the wider split gap. A larger gap results in a lower stored electrical energy within the split gap. Consequently, the displacement currents flowing through the resonant structure decrease, which weakens the induced current loops. Because the magnetic field in such metamaterial structures is directly generated by circulating loop currents, a reduction in current strength leads to a significantly lower magnetic field and potentially a decrease in effective inductance. This reduction in inductance, in turn, can influence the resonant behavior of the structure, according to the equation S5. This explains the sudden frequency jump observed.

REFERENCES

1. D. Isakov, C. J. Stevens, F. Castles, and P. S. Grant, "A split ring resonator dielectric probe for near-field dielectric imaging," Sci. reports **7**, 2038 (2017).
2. Y. Fu, W. Fan, H. Jin, and Q. Chen, "A new capacitance angle sensor of concentric ring multi-layer differential," Measurement **158**, 107625 (2020).